Massachusetts Institute of Technology

MAIN-BELT COMET P/2012 T1 (PANSTARRS)[*]

Henry H. Hsieh[1,7], Heather M. Kaluna[1,8], Bojan Novaković[2], Bin Yang[1,8], Nader Haghighipour[1,8], Marco Micheli[1], Larry Denneau[1], Alan Fitzsimmons[3], Robert Jedicke[1], Jan Kleyna[1,8], Peter Vereš[1], Richard J. Wainscoat[1], Megan Ansdell[1,8], Garrett T. Elliott[1], Jacqueline V. Keane[1,8], Karen J. Meech[1,8], Nicholas A. Moskovitz[4], Timm E. Riesen[1,8], Scott S. Sheppard[5], Sarah Sonnett[1], David J. Tholen[1], Laurie Urban[1,8], Nick Kaiser[1], K. C. Chambers[1], William S. Burgett[1], Eugene A. Magnier[1], Jeffrey S. Morgan[1], and Paul A. Price[6]

[1] Institute for Astronomy, University of Hawaii, 2680 Woodlawn Drive, Honolulu, HI 96822, USA; hsieh@ifa.hawaii.edu
[2] Department of Astronomy, Faculty of Mathematics, University of Belgrade, Studentski trg 16, 11000 Belgrade, Serbia
[3] Astrophysics Research Centre, Queens University Belfast, Belfast BT7 1NN, UK
[4] Department of Earth, Atmospheric, & Planetary Sciences, Massachusetts Institute of Technology, 77 Massachusetts Avenue, Cambridge, MA 02139, USA
[5] Department of Terrestrial Magnetism, Carnegie Institution of Washington, 5241 Broad Branch Road, NW, Washington, DC 20015, USA
[6] Department of Astrophysical Sciences, Peyton Hall, Princeton University, Princeton, NJ 08544, USA

ABSTRACT

We present initial results from observations and numerical analyses aimed at characterizing the main-belt comet P/2012 T1 (PANSTARRS). Optical monitoring observations were made between 2012 October and 2013 February using the University of Hawaii 2.2 m telescope, the Keck I telescope, the Baade and Clay Magellan telescopes, Faulkes Telescope South, the Perkins Telescope at Lowell Observatory, and the Southern Astrophysical Research Telescope. The object's intrinsic brightness approximately doubles from the time of its discovery in early October until mid-November and then decreases by ∼60% between late December and early February, similar to photometric behavior exhibited by several other main-belt comets and unlike that exhibited by disrupted asteroid (596) Scheila. We also used Keck to conduct spectroscopic searches for CN emission as well as absorption at $0.7\,\mu$m that could indicate the presence of hydrated minerals, finding an upper limit CN production rate of $Q_{\mathrm{CN}} < 1.5 \times 10^{23}$ mol s^{-1}, from which we infer a water production rate of $Q_{\mathrm{H_2O}} < 5 \times 10^{25}$ mol s^{-1}, and no evidence of the presence of hydrated minerals. Numerical simulations indicate that P/2012 T1 is largely dynamically stable for >100 Myr and is unlikely to be a recently implanted interloper from the outer solar system, while a search for potential asteroid family associations reveals that it is dynamically linked to the ∼155 Myr old Lixiaohua asteroid family.

Key words: comets: general – minor planets, asteroids: general

Online-only material: color figures

1. INTRODUCTION

Main-belt comets (MBCs; Hsieh & Jewitt 2006) exhibit cometary activity indicative of sublimating ice, yet orbit entirely within the main asteroid belt (Figure 1). Seven MBCs—133P/Elst-Pizarro, 176P/LINEAR, 238P/Read, 259P/Garradd, P/2010 R2 (La Sagra), P/2006 VW$_{139}$, and P/2012 T1 (PANSTARRS)—are currently known. In addition, three other objects—P/2010 A2 (LINEAR), (596) Scheila, and P/2012 F5 (Gibbs)—have been observed to exhibit comet-like dust emission, though their active episodes have been attributed to impact events and are not believed to be sublimation-driven (Jewitt et al. 2010, 2011; Snodgrass et al. 2010; Bodewits et al. 2011; Ishiguro et al. 2011; Stevenson et al. 2012). As such, we do not consider these objects to be ice-bearing main-belt objects, and refer to them as disrupted asteroids (Figure 1).

2. OBSERVATIONS

P/2012 T1 was discovered on 2012 October 6 by the 1.8 m Pan-STARRS1 (PS1) survey telescope on Haleakala (Wainscoat et al. 2012). PS1 employs a 3°.2 × 3°.2 1.4 gigapixel camera, consisting of 60 orthogonal transfer arrays, each comprising 64 590 × 598 pixel CCDs. Our discovery observations were made using Sloan Digital Sky Survey (SDSS) r'- and i'-like filters designated r_{P1} and i_{P1} (Tonry et al. 2012). Comet candidate identification in PS1 data is accomplished using automated point-spread function analysis procedures (Hsieh et al. 2012b) implemented as part of PS1's Moving Object Processing System (Denneau et al. 2013).

Follow-up observations were obtained in photometric conditions between 2012 October and 2013 February using the University of Hawaii (UH) 2.2 m and the 10 m Keck I telescopes, both on Mauna Kea, the 6.5 m Baade and Clay Magellan telescopes at Las Campanas, the 2.0 m Faulkes Telescope South (FTS) at Siding Spring, the 1.8 m Perkins Telescope (PT) at Lowell Observatory, and the Southern Astrophysical Research (SOAR) telescope on Cerro Pachon (Table 1; Figures 2(a) and (b)). We employed a 2048 × 2048 pixel Textronix CCD for UH observations, the Low Resolution Imaging Spectrometer (LRIS; Oke et al. 1995) for Keck observations, the Inamori Magellan Areal Camera and Spectrograph for Baade observations, the Megacam mosaic camera (consisting of 36 2048×4608 pixel CCDs) for Clay observations, a 4096 × 4096 pixel Fairchild
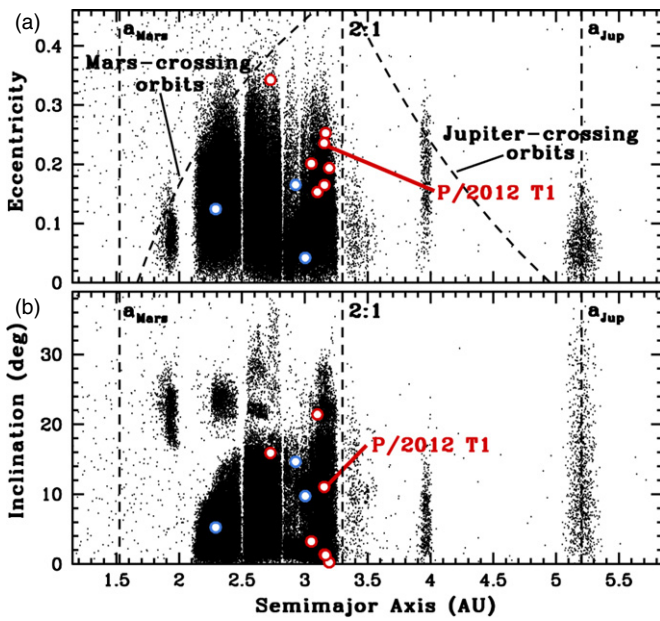
Figure 1. Semimajor axis vs. (a) eccentricity and (b) inclination plots for probable MBCs (red circles) and disrupted asteroids (blue circles).
(A color version of this figure is available in the online journal.)

CCD for FTS observations, the Perkins ReImaging System for Lowell observations, and the SOAR Optical Imager (Schwarz et al. 2004) for SOAR observations. We used SDSS-like filters for Clay observations, Bessell filters for FTS observations, and Kron–Cousins filters for all other observations. UH 2.2 m, Keck, Lowell, and SOAR observations were conducted using non-sidereal tracking at the apparent rate and direction of motion of P/2012 T1 on the sky, while other observations were conducted using sidereal tracking.

PS1 data were reduced using the system's Image Processing Pipeline (Magnier 2006). We performed bias subtraction and

flat-field reduction for follow-up data using Image Reduction and Analysis Facility (IRAF; Tody 1986) software and using flat fields constructed either from images of the illuminated interior of the telescope dome or dithered images of the twilight sky. Some photometric calibration was performed using field star magnitudes provided by the SDSS (York et al. 2000) converted to Kron–Cousins R-band equivalents using the transformation equations derived by R. Lupton (available online at http://www.sdss.org/). Photometry of Landolt (1992) standard stars and field stars was performed for all data using IRAF and obtained by measuring net fluxes within circular apertures, with background sampled from surrounding circular annuli. Conversion of r'-band magnitudes measured from PS1 and Clay data to their R-band equivalents was performed assuming approximately solar colors for the object.

Comet photometry was performed using circular apertures, where, to avoid dust contamination from the comet itself, background sky statistics are measured manually in regions of blank sky near, but not adjacent, to the object. Photometry aperture sizes were chosen to encompass >95% of the total flux from the comet (coma and tail) while minimizing interference from nearby field stars or galaxies, and varied from 3″.0 to 10″.0 in radius depending on seeing conditions. Field stars in comet images were also measured to correct for any extinction variations during each night.

In addition to imaging, we also obtained optical spectra of P/2012 T1 on 2012 October 19 with LRIS in spectroscopic mode on Keck. Two G2V solar analog stars, HD28099 and HD19061, were also observed to allow removal of atmospheric absorption features and calculation of P/2012 T1's relative reflectance spectrum. We utilized a 1″.0-wide long-slit mask and LRIS's D500 dichroic, with a 400/3400 grism on the blue side (dispersion of 1.09 Å pixel^{-1} and spectral resolution of ∼7 Å), and 150/7500 grating on the red side (dispersion of 3.0 Å pixel^{-1} and spectral resolution of ∼18 Å). Exposure times totaled 1320 s and 1200 s on the blue and red sides,
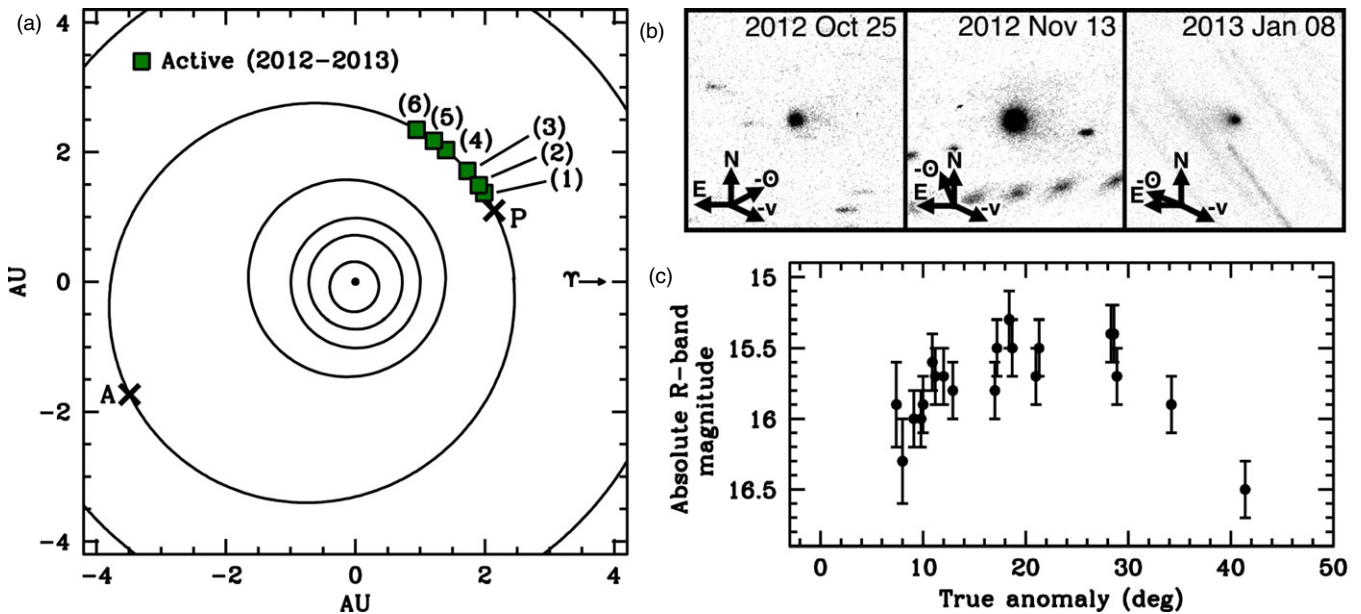
Figure 2. (a) Orbital position plot with the Sun (black dot) at the center, and the orbits of Mercury, Venus, Earth, Mars, P/2012 T1, and Jupiter shown as black lines. Perihelion (P) and aphelion (A) are marked with crosses. Green squares correspond to observations from (1) 2012 October 6–8, (2) 2012 October 12–25, (3) 2012 November 8–14, (4) 2012 December 18–20, (5) 2013 January 8, and (6) 2013 February 4. (b) Composite images of P/2012 T1 (center of each panel). In each panel, north (N), east (E), and the antisolar (−⊙) and negative heliocentric velocity (−v) directions are marked. (c) Plot of absolute magnitude vs. true anomaly for observations listed in Table 1.
(A color version of this figure is available in the online journal.)

Table 1
Observations

UT Date	Tel.[a]	N[b]	t[c]	Filter	ν[d]	R[e]	Δ[f]	α[g]	PA$_{-\odot}$[h]	PA$_{-v}$[i]	α_{pl}[j]	$m_R(R,\Delta,\alpha)$[k]	$m_R(1,1,0)$[l]	$Af\rho$[m]
2012 Sep 11	Perihelion.........................				0.0	2.411	1.753	21.4	262.1	243.5	6.3	⋯	⋯	⋯
2012 Oct 06	PS1	1	40	r_{P1}	7.4	2.414	1.540	14.4	273.5	244.1	6.8	19.6 ± 0.1	15.9 ± 0.3	10.1 ± 2.9
2012 Oct 08	PS1	1	40	r_{P1}	8.0	2.415	1.527	13.7	274.9	244.1	6.8	19.9 ± 0.1	16.3 ± 0.3	8.0 ± 2.3
2012 Oct 12	Clay	38	2280	r'	9.1	2.416	1.507	12.4	278.1	244.2	6.7	19.59 ± 0.02	16.0 ± 0.2	9.3 ± 1.7
2012 Oct 14	UH2.2	1	300	R	9.8	2.418	1.496	11.5	280.3	244.3	6.6	19.49 ± 0.05	16.0 ± 0.2	11.1 ± 2.1
2012 Oct 15	UH2.2	2	600	R	10.0	2.418	1.491	11.2	281.4	244.3	6.6	19.36 ± 0.05	15.9 ± 0.2	11.5 ± 2.4
2012 Oct 15	FTS	8	480	R	10.0	2.418	1.491	11.1	281.6	244.3	6.6	19.40 ± 0.06	15.9 ± 0.2	13.1 ± 2.2
2012 Oct 18	Keck	4	1440	B	10.9	2.419	1.479	10.0	285.3	244.4	6.4	20.17 ± 0.02	⋯	⋯
		4	1200	R	⋯	⋯	⋯	⋯	⋯	⋯	⋯	19.03 ± 0.03	15.6 ± 0.2	12.5 ± 2.3
2012 Oct 19	Keck	4	1440	B	11.2	2.419	1.475	9.7	286.8	244.4	6.4	20.23 ± 0.02	⋯	⋯
		4	1200	R	⋯	⋯	⋯	⋯	⋯	⋯	⋯	19.11 ± 0.02	15.7 ± 0.2	12.4 ± 2.3
2012 Oct 22	UH2.2	14	4200	R	12.0	2.421	1.466	8.5	292.0	244.5	6.2	19.01 ± 0.02	15.7 ± 0.2	11.4 ± 2.1
2012 Oct 25	Baade	3	180	B	12.9	2.422	1.459	7.6	298.2	244.5	6.0	19.98 ± 0.06	⋯	⋯
		2	120	V	⋯	⋯	⋯	⋯	⋯	⋯	⋯	19.33 ± 0.04	⋯	⋯
		5	300	R	⋯	⋯	⋯	⋯	⋯	⋯	⋯	19.05 ± 0.03	15.8 ± 0.2	11.4 ± 2.1
2012 Nov 8	UH2.2	2	600	R	17.0	2.431	1.455	5.3	0.5	244.8	4.8	18.98 ± 0.04	15.8 ± 0.2	13.0 ± 2.4
2012 Nov 9	UH2.2	2	1200	R	17.2	2.432	1.457	5.4	5.5	244.8	4.7	18.69 ± 0.03	15.5 ± 0.2	12.2 ± 2.3
2012 Nov 13	UH2.2	26	7800	R	18.4	2.434	1.467	6.3	22.6	244.8	4.2	18.57 ± 0.02	15.3 ± 0.2	12.8 ± 2.4
2012 Nov 14	UH2.2	14	4200	R	18.7	2.435	1.470	6.5	26.1	244.8	4.1	18.76 ± 0.02	15.5 ± 0.2	12.7 ± 2.4
2012 Nov 22	Lowell	4	2400	R	21.0	2.441	1.502	9.1	44.9	244.7	3.1	19.11 ± 0.03	15.7 ± 0.2	13.1 ± 2.4
2012 Nov 23	Lowell	2	1400	R	21.3	2.442	1.507	9.5	43.9	244.7	3.0	18.95 ± 0.04	15.5 ± 0.2	15.5 ± 2.9
2012 Dec 18	UH2.2	30	9000	R	28.3	2.467	1.712	17.7	64.5	244.1	−0.1	19.47 ± 0.02	15.4 ± 0.2	10.6 ± 2.0
2012 Dec 19	UH2.2	49	15000	R	28.6	2.468	1.723	17.9	64.8	244.1	−0.2	19.48 ± 0.02	15.4 ± 0.2	11.0 ± 2.0
2012 Dec 20	Lowell	4	4800	R	28.9	2.470	1.734	18.2	65.1	244.1	−0.3	19.82 ± 0.04	15.7 ± 0.2	9.5 ± 1.8
2013 Jan 08	UH2.2	10	8400	R	34.2	2.493	1.962	21.6	69.5	243.7	−2.1	20.40 ± 0.02	15.9 ± 0.2	8.2 ± 1.5
2013 Feb 04	SOAR	1	600	R	41.4	2.531	2.334	22.9	73.3	243.9	−3.5	21.41 ± 0.05	16.5 ± 0.2	6.0 ± 1.1
2015 Jun 27	Aphelion.........................				180.0	3.896	3.656	15.0	114.2	296.1	0.5	⋯	⋯	⋯
2018 Apr 12	Perihelion.........................				0.0	2.402	3.392	3.1	134.3	243.4	−2.9	⋯	⋯	⋯

Notes.
[a] Telescope.
[b] Number of exposures.
[c] Total integration time, in s.
[d] True anomaly, in degrees.
[e] Heliocentric distance of object, in AU.
[f] Geocentric distance of object, in AU.
[g] Solar phase angle (Sun–object–Earth), in degrees.
[h] Position angle of the antisolar vector, in degrees east of north.
[i] Position angle of the negative velocity vector, in degrees east of north.
[j] Orbit plane angle, in degrees.
[k] Mean apparent R-band magnitude.
[l] Absolute R-band magnitude (at $R = \Delta = 1$ AU and $\alpha = 0°$), assuming solar colors and IAU H, G phase-darkening where $G = 0.15$. Listed uncertainties are dominated by the estimated uncertainty in G.
[m] Dust contribution (computed using 5″.0 photometry apertures), as parameterized by A'Hearn et al. (1984), in cm.

respectively, where the comet was at an air mass of ∼1.2 during our observations. Data reduction was performed using IRAF.

3. RESULTS AND ANALYSIS

3.1. Photometric Analysis

Photometry results from follow-up observations are listed in Table 1. For reference, we also compute $Af\rho$ (A'Hearn et al. 1984) for each of our observations, though we note that it is not always a reliable measurement of the dust contribution to comet photometry in cases of non-spherically symmetric comae (e.g., Fink & Rubin 2013).

While much of our photometry are based on snapshot observations (meaning that unknown brightness variations due to nucleus rotation could be present), we find that the object's intrinsic brightness roughly doubles from the time of its discovery in early October until mid-November (∼40 days; over a true anomaly range of $7° < \nu < 20°$), and then decreases by ∼60% between late December and early February (∼50 days; $28° < \nu < 42°$; Figure 2(c)). Similar photometric behavior is observed for several other MBCs (Hsieh et al. 2012b, 2012c). For comparison, the brightness of disrupted asteroid (596) Scheila declined by 30% in just 8 days (Jewitt et al. 2011). MBCs 133P and 238P both exhibited long-lived brightening and did so during multiple apparitions, making us extremely confident in their cometary natures (Hsieh et al. 2004, 2010, 2011). While long-lived activity is no guarantee of cometary activity (Hsieh et al. 2012a), the photometric behavior of P/2012 T1 is certainly inconsistent with dust particles ejected impulsively in an impact. Its steady brightening implies the action of a prolonged dust ejection mechanism like sublimation. Furthermore, while apparently long-lived activity could be due to the long dissipation times of large particles ejected by an impact, P/2012 T1's eventual fading after several weeks suggests that this is not the case here, since such large particles would be expected to persist much longer (cf. Hsieh et al. 2004; Jewitt et al. 2010).
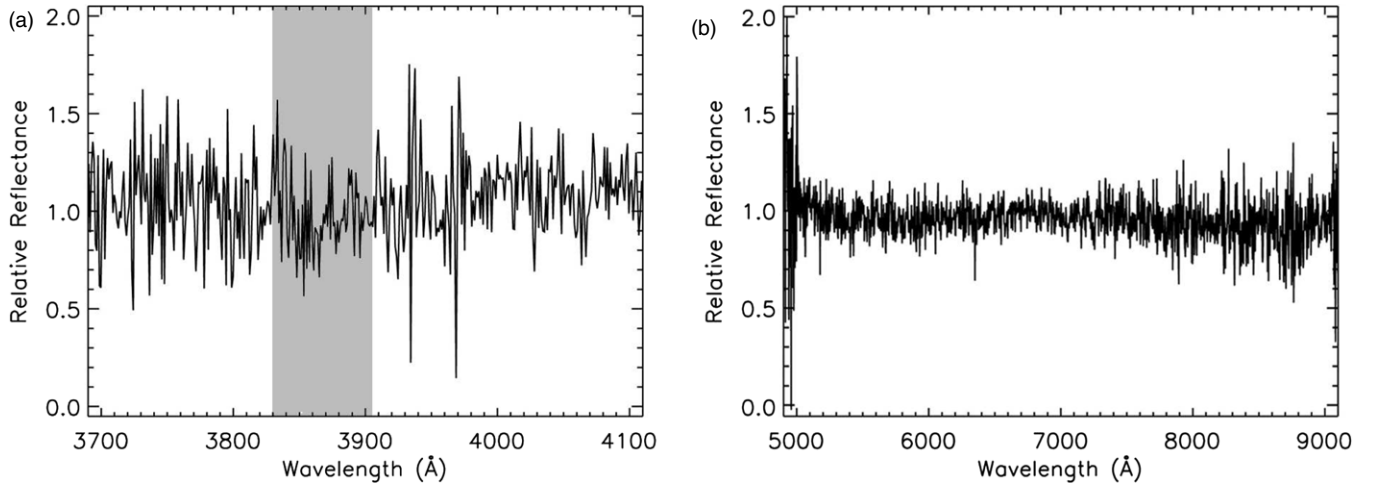
Figure 3. Relative reflectance spectra of P/2012 T1 obtained with LRIS on Keck I on 2012 October 19 from (a) 3700 Å–4100 Å, where the shaded region indicates the wavelength region where the CN emission band is expected, and (b) 5000 Å–9000 Å, where absorption at 0.7 μm due to a charge transfer transition in oxidized iron is expected if hydrated minerals are present.

Multi-filter observations using LRIS on Keck I (which permits simultaneous B- and R-band imaging, eliminating the effects of rotational brightness variations) and the Baade telescope indicates that coma of P/2012 T1 had approximately solar colors of $B - R = 1.13 \pm 0.04$ (measured on Keck), and $B - V = 0.65 \pm 0.07$ and $V - R = 0.37 \pm 0.05$ (measured on Baade).

3.2. Spectroscopic Analysis

Our LRIS red-side spectrum (Figure 3) of P/2012 T1 is approximately linear with a slightly blue slope of $-1.5\% \pm 1.0\%/1000$ Å, similar to the spectrum of 133P when it was active during its 2007 perihelion passage (Licandro et al. 2011). This result differs significantly, however, from the red slopes measured for MBC P/2006 VW$_{139}$ when it was active (7.2%/1000 Å; Hsieh et al. 2012b) as well as for other cometary dust comae (Kolokolova et al. 2004).

To derive the CN production rate (cf. Hsieh et al. 2012a; Jewitt & Guilbert-Lepoutre 2012), we employ a simple Haser (1957) model, using a resonance fluorescence efficiency of $g[1 \text{ AU}] = 3.63 \times 10^{-13}$ erg s^{-1} molecule^{-1} (Schleicher 2010). We find an upper limit to the CN production rate of $Q_{CN} < 1.5 \times 10^{23}$ mol s^{-1}. The CN to water production rate in MBCs is unknown, but we adopt the average ratio in other observed comets ($\log[Q_{CN}/Q_{OH}] \sim -2.5$; $Q_{OH}/Q_{H_2O} \sim 90\%$) (A'Hearn et al. 1995), and infer a water production rate of $Q_{H_2O} < 5 \times 10^{25}$ mol s^{-1}.

We also search for 0.7 μm absorption due to a charge transfer transition in oxidized iron in phyllosilicates, indicative of the presence of hydrated minerals (Vilas 1994). Thermal evolution models suggest that aqueous alteration occurred within asteroid parent body interiors (Cohen & Coker 2000; Wilson et al. 1999). If these models are correct, MBCs could be icy fragments from the outer shells of asteroid parent bodies where temperatures were never high enough to melt ice. If an MBC happened to be a fragment from near an ice and hydrated rock boundary in such a parent body, it could contain hydrated minerals. To date, no MBCs have shown evidence of having hydrated minerals on their surfaces. Our Keck spectrum of P/2012 T1 likewise shows no signs of absorption at 0.7 μm, and thus, no detectable evidence of hydrated minerals.

3.3. Dynamical Analysis

3.3.1. Stability Analysis

To determine whether P/2012 T1 is likely to be native to the main belt, or if it could be a recently implanted interloper from the outer solar system, we analyze its long-term dynamical stability in a manner similar to that performed for other MBCs (cf. Jewitt et al. 2009; Hsieh et al. 2012a, 2012b, 2012c). We generate 9 sets of 100 dynamical clones of P/2012 T1 that are Gaussian-distributed in orbital element space and centered on the object's osculating orbital elements as of 2012 December 1. Three of these sets are characterized by σ values equivalent to the uncertainties on those orbital elements ($\sigma_a = 3 \times 10^{-5}$ AU, $\sigma_e = 3 \times 10^{-5}$, $\sigma_i = 6^\circ \times 10^{-4}$), three sets are characterized by σ values 10 times larger than those uncertainties, and three sets are characterized by σ values 100 times larger. We then perform forward integrations for 100 Myr using the N-body integration package, Mercury (Chambers 1999). We include the gravitational effects of all eight major planets and treat all dynamical clones as massless test particles. Non-gravitational forces are not considered in this analysis.

In these simulations, less than 5% of the test particles reach heliocentric distances of >50 AU (and are therefore considered to have been ejected from the asteroid belt) over the 100 Myr test period. The remaining test particles diverge to occupy regions of orbital element space that are larger than their initial distributions but that are also essentially independent of those initial distributions, i.e., the 1σ sets of test particles diverge to occupy similar regions as the 100σ sets (Figure 4). This divergence occurs quickly (within 10^4 years) and remains approximately constant over the 100 Myr test period. We therefore find that P/2012 T1 is largely dynamically stable and is unlikely to be a recently implanted interloper, though we do note that the ejection of a small number of test particles indicates that the region is not perfectly stable over the considered time period.

3.3.2. Search for Associated Dynamical Families

MBCs 133P and P/2006 VW$_{139}$ have recently been found to be dynamical members of very young (<10 Myr) asteroid families (Nesvorný et al. 2008; Novaković et al. 2012). These

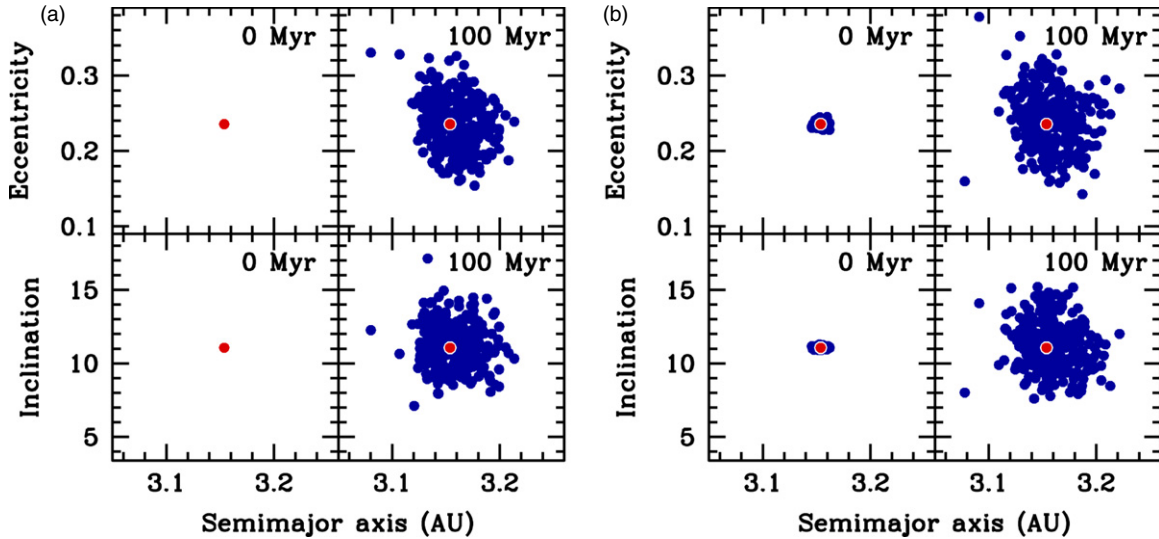**Figure 4.** Semimajor axis vs. eccentricity and inclination plots for (a) all 1σ sets of dynamical clones and (b) all 100σ sets of clones of P/2012 T1 integrated as described in Section 3.3.1, where the orbital elements of all clones (blue dots) are shown at the beginning (0 Myr) and at the end (100 Myr) of each integration. For reference, the original orbital elements of the object are marked with a red dot in each plot.
(A color version of this figure is available in the online journal.)

findings are interesting because the surfaces of ice-bearing main-belt objects may become significantly collisionally devolatilized on timescales of $\ll 1$ Gyr (Hsieh 2009). However, if MBCs only originated in the recent fragmentation events that created the aforementioned young families, their surfaces should have experienced far less collisional devolatilization, and thus remain susceptible to activation by small impactors (cf. Hsieh et al. 2004; Capria et al. 2012). While we currently lack a sufficient sample size to ascertain whether there is a significant over-abundance of MBCs in young families, the fact that two of seven MBCs ($\sim$30%) are found to belong to such families is suggestive of a physical correlation.

To test whether P/2012 T1 originated in a recent fragmentation event, we search for an associated dynamical family utilizing a hierarchical clustering analysis (Zappalà et al. 1990). Using computed proper elements of $a_p = 3.15967$ AU, $e_p = 0.19555$, and $\sin(i_p) = 0.17536$, we find that P/2012 T1 belongs to the $\sim$155 Myr old Lixiaohua asteroid family (Novaković et al. 2010). While the Lixiaohua family is of intermediate age, P/2012 T1 could belong to an even younger subfamily, much as the young Beagle and P/2006 VW$_{139}$ families are both subgroups of the much older Themis family (Nesvorný et al. 2008; Novaković et al. 2012). Unfortunately, the density of asteroids in the region of orbital element space occupied by the Lixiaohua family is extremely high. In fact, most Lixiaohua family members, including P/2012 T1, are linked to the family at cutoff velocities as low as 20 m s^{-1}. As such, identification of a younger subfamily for P/2012 T1 will be extremely difficult. The slight instability of the P/2012 T1's orbit (Section 3.3.1) also interferes with our ability to establish young family linkages using techniques such as those applied in the case of P/2006 VW$_{139}$ (Novaković et al. 2012).

4. DISCUSSION

Currently, the key question that must be answered when a main-belt object exhibits comet-like activity is whether that activity is sublimation-driven, implying the presence of ice, or is produced by another means. Definitive evidence of sublimation would be the direct detection of a gaseous sublimation product

such as CN or H$_2$O in the coma of such an object. Unfortunately, unsuccessful attempts to detect CN have now been made for four of the most recently discovered MBCs (Jewitt et al. 2009; Hsieh et al. 2012b, 2012c; Licandro et al. 2013; this work), where each work has found similar upper limit CN production rates of 10^{23}–10^{24} mol s^{-1}, corresponding to water production rates of $Q_{H_2O} < 10^{26}$ mol s^{-1}. Searches for line emission from the $(1_{10}$–$1_{01})$ rotational transition of ortho-water at 557 GHz with the *Herschel Space Observatory* for 176P and P/2012 T1 were also unsuccessful, finding $Q_{H_2O} < 4 \times 10^{25}$ mol s^{-1} and $Q_{H_2O} < 7 \times 10^{25}$ mol s^{-1}, respectively (de Val-Borro et al. 2012, L. O'Rourke et al. 2013, private communication). While these results do not definitively rule out sublimation, they do indicate that the production rates of sublimation products by MBCs are too low to detect from current Earth-bound facilities. As such, we must rely on indirect evidence to determine the likely source of comet-like activity in main-belt objects.

Jewitt (2012) examined various mechanisms by which an asteroid-like body could undergo comet-like mass loss, including ice sublimation, impact ejection, rotational instability, and electrostatic levitation, finding that in many individual cases of comet-like objects, the cause of observed mass loss could not be definitively identified due to insufficient observational data. Nonetheless, certain mechanisms could sometimes be ruled out based on physical and observational constraints.

For example, electrostatic levitation was ruled out as a cause of 133P's observed activity because it would have depleted the supply of mobile surface dust during a single active episode, leaving no obvious source of mobile dust for subsequent active episodes (Hsieh et al. 2004, 2010). The rapid rotation of 133P also minimizes the amount of electrostatic charging that can occur given the short time that any portion of the object's surface spends in sunlight (Hsieh et al. 2004). This mechanism's efficacy furthermore depends on unknown cohesive properties of asteroid regolith dust grains (Jewitt 2012). Finally, given the many asteroids similar to 133P with more favorable rotational properties, it is unclear why 133P would exhibit observable dust levitation while other asteroids do not. Dust ejection via rotational spin-up, perhaps via the Yarkovsky–O'Keefe–Radzievsky–Paddack effect (Rubincam 2000), was also ruled out due to the lack

of a plausible mechanism for producing repeated activity or explaining the rarity of similar activity on other asteroids.

Jewitt (2012) did note that for an object exhibiting repeated activity, sublimation appears to be the only reasonable explanation. Repeated activity has only been established for 133P and 238P, however, with others either failing to exhibit repeated activity upon completion of a full orbit period since its previously observed active episode (176P), or not yet having completed one full orbit since their first observed active episodes (259P, P/2010 R2, P/2006 VW$_{139}$, and P/2012 T1).

As discussed in Section 3.1, P/2012 T1's observed photometric behavior indicates ongoing and even increasing dust production over several weeks (Figure 2(c)), consistent with continuous sublimation-driven dust ejection and inconsistent with impulsive impact-driven dust ejection. The comet also exhibits a diffuse coma and a featureless fan-like tail that remains aligned with the antisolar direction, distinctly different from the crossed filamentary structure of P/2010 A2's tail, the three-plumed morphology of (596) Scheila's dust tail, and the orbit-plane-aligned dust trail of P/2012 F5 (Jewitt et al. 2010; Ishiguro et al. 2011; Stevenson et al. 2012; Moreno et al. 2012). The post-perihelion peaking of P/2012 T1's activity is also consistent with the post-perihelion peaking of activity for other MBCs (Hsieh et al. 2012c). While we cannot yet definitively conclude that P/2012 T1's activity is sublimation-driven, we note that all evidence examined thus far is consistent with sublimation. We therefore find that P/2012 T1 is most likely a true MBC, and not a disrupted asteroid, though additional observations (e.g., to search for repeated activity during its next perihelion passage in mid-2018) and more detailed dust modeling will be required to definitively rule out other dust ejection mechanisms.

A primary ultimate objective of MBC studies is to connect observations of the distribution and composition of volatiles in small primitive bodies to the distribution of volatiles in the protoplanetary disk, and to link this through disk observations to other forming planetary systems (Pontoppidan et al. 2010). Presently, we have insufficient information to make these connections, in part because we have few direct constraints on the volatile content of small bodies and because our solar system's precise dynamical history remains poorly understood. Further work on both fronts would help this situation, though significantly advancing our understanding of volatile material in the asteroid belt may require in situ investigation, e.g., by a visiting spacecraft.

REFERENCES

A'Hearn, M. F., Millis, R. L., Schleicher, D. G., Osip, D. J., & Birch, P. V. 1995, Icar, 118, 223
A'Hearn, M. F., Schleicher, D. G., Millis, R. L., Feldman, P. D., & Thompson, D. T. 1984, AJ, 89, 579
Bodewits, D., Kelley, M. S., Li, J.-Y., et al. 2011, ApJL, 733, L3
Capria, M. T., Marchi, S., De Sanctis, M. C., Coradini, A., & Ammannito, E. 2012, A&A, 537, A71
Chambers, J. E. 1999, MNRAS, 304, 793
Cohen, B. A., & Coker, R. F. 2000, Icar, 145, 369
Denneau, L., Jedicke, R., Grav, T., et al. 2013, PASP, 125, 357
de Val-Borro, M., Rezac, L., Hartogh, P., et al. 2012, A&A, 546, L4
Fink, U., & Rubin, M. 2013, Icar, 221, 721
Haser, L. 1957, BSRSL, 43, 740
Hsieh, H. H. 2009, A&A, 505, 1297
Hsieh, H. H., & Jewitt, D. 2006, Sci, 312, 561
Hsieh, H. H., Jewitt, D., & Fernández, Y. R. 2004, AJ, 127, 2997
Hsieh, H. H., Jewitt, D., Lacerda, P., Lowry, S. C., & Snodgrass, C. 2010, MNRAS, 403, 363
Hsieh, H. H., Meech, K. J., & Pittichová, J. 2011, ApJL, 736, L18
Hsieh, H. H., Yang, B., & Haghighipour, N. 2012a, ApJ, 744, 9
Hsieh, H. H., Yang, B., Haghighipour, N., et al. 2012b, ApJL, 748, L15
Hsieh, H. H., Yang, B., Haghighipour, N., et al. 2012c, AJ, 143, 104
Ishiguro, M., Hanayama, H., Hasegawa, S., et al. 2011, ApJL, 741, L24
Jewitt, D. 2012, AJ, 143, 66
Jewitt, D., & Guilbert-Lepoutre, A. 2012, AJ, 143, 21
Jewitt, D., Weaver, H., Agarwal, J., Mutchler, M., & Drahus, M. 2010, Natur, 467, 817
Jewitt, D., Weaver, H., Mutchler, M., Larson, S., & Agarwal, J. 2011, ApJL, 733, L4
Jewitt, D., Yang, B., & Haghighipour, N. 2009, AJ, 137, 4313
Kolokolova, L., Hanner, M. S., Levasseur-Regourd, A.-C., & Gustafson, B. Å. S. 2004, in Comets II, ed. M. C. Festou, H. U. Keller, & H. A. Weaver (Tucson, AZ: Univ. Arizona Press), 577
Landolt, A. U. 1992, AJ, 104, 340
Licandro, J., Campins, H., Tozzi, G. P., et al. 2011, A&A, 532, A65
Licandro, J., Moreno, F., de León, J., et al. 2013, A&A, 550, A17
Magnier, E. 2006, in Proc. Advanced Maui Optical and Space Surveillance Technologies Conference, ed. S. Ryan (Kihei, HI: The Maui Economic Development Board), E5
Moreno, F., Licandro, J., & Cabrera-Lavers, A. 2012, ApJL, 761, L12
Nesvorný, D., Bottke, W. F., Vokrouhlický, D., et al. 2008, ApJL, 679, L143
Novaković, B., Hsieh, H. H., & Cellino, A. 2012, MNRAS, 424, 1432
Novaković, B., Tsiganis, K., & Knežević, Z. 2010, MNRAS, 402, 1263
Oke, J. B., Cohen, J. G., Carr, M., et al. 1995, PASP, 107, 375
Pontoppidan, K. M., Salyk, C., Blake, G. A., et al. 2010, ApJ, 720, 887
Rubincam, D. P. 2000, Icar, 148, 2
Schleicher, D. G. 2010, AJ, 140, 973
Schwarz, H. E., Ashe, M. C., Boccas, M., et al. 2004, Proc. SPIE, 5492, 564
Snodgrass, C., Tubiana, C., Vincent, J.-B., et al. 2010, Natur, 467, 814
Stevenson, R., Kramer, E. A., Bauer, J. M., Masiero, J. R., & Mainzer, A. K. 2012, ApJ, 759, 142
Tody, D. 1986, Proc. SPIE, 627, 733
Tonry, J. L., Stubbs, C. W., Lykke, K. R., et al. 2012, ApJ, 750, 99
Vilas, F. 1994, Icar, 111, 456
Wainscoat, R., Hsieh, H., Denneau, L., et al. 2012, CBET, 3252, 1
Wilson, L., Keil, K., Browning, L. B., Krot, A. N., & Bourcier, W. 1999, M&PS, 34, 541
York, D. G., Adelman, J., Anderson, J. E., Jr., et al. 2000, AJ, 120, 1579
Zappalà, V., Cellino, A., Farinella, P., & Knežević, Z. 1990, AJ, 100, 2030